Surface Science 299/300 (1994) 965–979
North-Holland

surface science

Scanning tunneling spectroscopy

Randall M. Feenstra
IBM Research Division, T.J. Watson Research Center, Yorktown Heights, NY 10598, USA

Received 4 May 1993; accepted for publication 1 June 1993

The development of the field of spectroscopic measurement with the scanning tunneling microscope (STM) is discussed. A historical review of early experimental results in this field is presented, with emphasis on the techniques for data acquisition and interpretation. The applicability of STM spectroscopic measurement to surface structural determination is addressed. The role of geometric versus electronic contributions to STM images is discussed, with reference to studies of Si(111)7 × 7, Si(111)2 × 1, and Ge(111)c(2 × 8) surfaces. It is concluded that, for semiconductor surfaces, the observed corrugations are dominated by electronic effects. Issues of dynamic range in spectroscopic measurement, and interpretation of spectroscopic images, are examined.

1. Introduction

Since its inception in 1982, the scanning tunneling microscope (STM) [1–3] has proven to be a powerful tool within the field of surface science. When used in a spectroscopic mode, the STM can probe the electronic states of a surface which are located within a few eV on either side of the Fermi level. Since this energy range is typical for surface states derived from dangling bonds on semiconductor surfaces, STM spectroscopic studies have focused primarily on those materials. Indeed, since STM images of semiconductor surface structures often depend sensitively on the voltage applied between the probe-tip and sample, it is generally necessary to perform some sort of spatially resolved spectroscopic measurement in order to deduce the geometric structure of the surface.

This article presents a historical perspective of the development of scanning tunneling spectroscopy techniques. The development of the STM and various other related methods are discussed in the preceding article by Rohrer [51]. Here, we focus on the specific application of the STM to spectroscopic studies primarily of semiconductor surfaces. There was a period of intense activity in this area in the years 1985–1987, with a number of research groups developing various techniques for acquiring and analyzing the data. We review these "early" results here in chronological order, including discussion of the applicability and relative merits of the methods. For simplicity we concentrate on the early experimental works with the STM, although, as referred to briefly throughout this paper, significant theoretical works also existed and in many cases they predated the experimental studies.

Before embarking on our historical survey of this field, it is important to put in perspective the level of knowledge which determined the course of many of the STM spectroscopic studies. In the early 1980's, a large number of reconstructions of semiconductor surfaces were known to exist, and had been characterized in many cases by diffraction and scattering methods. However, the detailed arrangement of atoms which constituted these surface structures were, in general, not definitively known. Many models had been proposed for each particular surface structure, but deciding amongst these models on the basis of available data was difficult. Into this arena came the STM [1–3] providing beautiful images of, e.g., the Si(111)7 × 7 surface with atomic resolution [4,5], and it seemed that the entire problem of surface structure determination would soon be

SSDI 0039-6028(93)E0379-9

solved. However, the situation proved to be somewhat more difficult – the STM images did not always directly lead to a unique surface structure due to limitations of resolution and/or the fact that the images themselves would depend on the applied voltage between the probe-tip and the sample. This voltage dependence is, of course, the essence of the spectroscopic capabilities of the STM, and thus can be regarded as a very useful aspect of the instrument. But, from the standpoint of determining surface structure, the voltage dependence of the STM was an unwanted complication and preferably something which could be ignored. Thus, it was all too easy to simply forget about the voltage dependence, and assume simply that the STM directly revealed the atoms on the surface. Such an assumption was at times adopted by both STM experts and nonexperts alike, and in some cases led to incorrect determinations of a surface structure. Finally, enough structures were correctly determined with the STM (and by other methods) so that some experience and intuition were gained which could be used to point the way through potential pitfalls in structural determination by STM. In short, the problem of surface structural determination, although it provides only one small application of STM spectroscopy, dominated much of the early work in the field.

It is probably worth discussing at this point one other general aspect of the STM which is important for both imaging and spectroscopic measurements, that is, the properties of the probe-tip. It is well known that the shape of the probe-tip apex can dramatically influence the appearance of STM images; on the atomic scale, individual corrugation maxima may be elongated in a particular direction by an asymmetric tip, or effects of multiple tips can distort and complicate the images. Similarly, the electronic properties of a probe-tip can influence spectroscopic measurements, leading to apparent band gaps or voltage offsets around zero volts, or in worse cases to distinct features in the spectrum. Such effects were fully appreciated in the early works. Efforts were made to clean the tips to ensure good metallic character, and enough spectroscopy data were collected using different tips and samples so that individual spurious results could be discarded. Indeed, an inspection of the results in the early works reveals many of the highest quality spectra which have been reported to date, and most of the results have been reproduced many times in later studies. Thus, probe-tip characteristics, although they do present a difficulty in spectroscopic studies, do not represent a limitation which cannot be overcome with sufficient careful work. On the other hand, it is apparent from the number of publications that the growth of the STM spectroscopic field has been somewhat slower than other areas of STM, and one reason for this may be the stringent demands of probe-tip cleanliness required for spectroscopic work.

2. Historical survey

2.1. Conductance spectroscopy and imaging

The basic mode of operation of the STM is constant-current imaging, in which the probe-tip is raster scanned across the surface and a feedback loop adjusts the height of the tip in order to keep the tunnel current constant. The resulting tip height, s, as a function of lateral (x, y) position, constitutes a constant-current image (often called a topograph). Within this same mode of STM operation, one can envision positioning the probe-tip at some fixed lateral position, and then ramping the bias voltage between tip and sample while keeping the tunnel current constant. The resultant s–V curve contains information on the spectrum of states over the applied voltage range. This type of measurement was first performed by Binnig and Rohrer, for the case of metal surfaces [3]. At high voltages > 4 V they observed a series of plateaus in the s–V curves. These features were interpreted in terms field-emission resonances consisting of standing waves formed in the positive electron energy region between the top of the triangular vacuum barrier and the sample surface. This observation provided important proof of the coherent nature of the tunneling between tip and sample, which, together with the exponential decay of the tunnel current [1] demonstrated that the STM did indeed operate

in a well-defined vacuum tunneling mode. Later measurements of field-emission resonances were performed by Becker, Golovchenko and Swartzentruber [6], who improved the spectral resolution by measuring conductance, dI/dV, using a modulation technique.

In addition to the field-emission resonances seen at high voltages in conductance spectra, weaker structure was observed at voltages < 4 V. This low voltage structure was identified as arising from image states in one study [7]. The first work to relate such spectral features with structurally derived electronic surface states was performed by Becker and co-workers, on the Si(111)7×7 surface [8]. Fig. 1a shows a topograph of the 7×7 structure, with the unit cell consisting of two equilateral triangles. Conductance spectra acquired over the two halves of the unit cell are shown in Fig. 2. The features labelled I and II in the spectra arise from surface states, whereas the oscillations at higher voltage arise from the above-mentioned field-emission resonances. At the time of this study, some asymmetry between the two halves of the 7×7 unit cell had already been reported in previous STM studies [4,5,9], although a quantitative measure of the voltage dependence of this effect was lacking. The observed asymmetry had been interpreted [9] in terms of the faulted and unfaulted halves of the 7×7 structure which appear in the dimer–adatom–stacking fault (DAS) model of this surface [10]. Thus, the two spectra in Fig. 2 are labelled according to which half of the unit cell they were acquired over. A clear difference between the spectra is seen, with the peak labelled II for the faulted-side spectrum being absent from the unfaulted side, and the peak labelled I being shifted between the spectra. Peak II was thus assigned to a specific electronic feature associated with the stacking fault in the DAS structure.

Imaging of these spectral features of the Si(111)7×7 unit cell was performed by recording the conductance signal, at a fixed voltage, simultaneously with the topography. The result is shown in Fig. 1b, for a sample bias of 2.0 V. The two halves of the unit cell, A and B, refer to the faulted and unfaulted sides of the structure re-

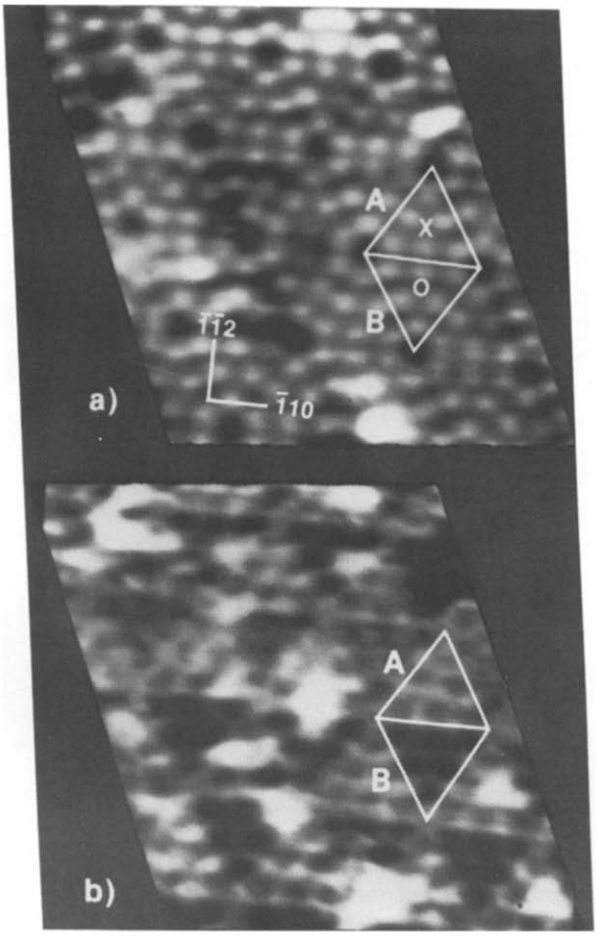

Fig. 1. (a) Grey-scale constant-current STM image of the Si(111)7×7 surface. Light areas are high, while dark areas are low, with a total range of 1 Å. (b) Simultaneous conductance image with light representing increased signal and dark representing decreased signal (arbitrary units). The 7×7 unit mesh is depicted as a rhombus built up from two equilateral triangles. The surface orientation is as shown, with the A and B designating triangular subunits with vertices pointing in the $\langle 2\bar{1}\bar{1} \rangle$ and $\langle \bar{2}11 \rangle$ directions, respectively. The points x and o indicate the centers of the subunits. (From Ref. [8].)

spectively according to the DAS model. In Fig. 1b, the faulted half appears brighter in the conductance, consistent with the spectra in Fig. 2 which show higher conductance at 2.0 V for the faulted spectrum.

In the above example of conductance imaging, the voltage of 2.0 V sample bias was specifically chosen to correspond to a large spectral feature (peak I) which forms the basis for the spectral

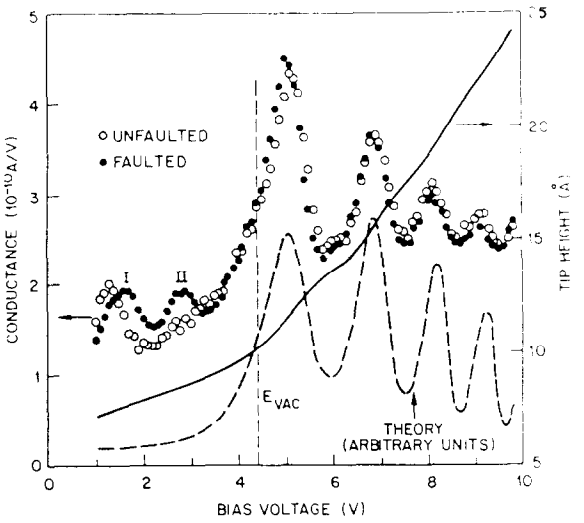

Fig. 2. Conductance spectra vs. sample bias voltage for the Si(111)7×7 surface. The filled circles and open circles denote data taken with the tip centered over faulted and unfaulted triangular subunits, respectively. The solid line shows the vacuum gap during the conductance measurements. The vacuum level is indicated, with the dashed curve showing the theoretical standing-wave conductance oscillations for the observed dependence on vacuum gap on bias voltage. (From Ref. [8].)

image. This procedure illustrates a general point regarding conductance imaging: it is always necessary to have detailed knowledge of the spectrum prior to choosing the specific imaging voltage, since otherwise the conductance image may just reflect some underlying "background" feature of the spectrum as opposed to a specific surface state feature. The same conclusion can be made for all the types of spectroscopic imaging, discussed below.

2.2. Constant-separation spectroscopy

The above examples of conductance spectroscopy and imaging, while providing clear and distinct spectroscopic results, suffer from the drawback that the measurements must be performed for only positive or negative tip–sample bias, but not both in the same scan. The reason for this limitation is that the tunnel current is kept constant during the scan, and crossing zero volts would result in tip–sample contact. The first study to overcome this limitation was performed by Feenstra, Thompson, and Fein, in which they acquired tunneling spectra at constant tip–sample separation using an interrupted feedback method [11]. Fig. 3 shows the resulting current–voltage (I–V) curve, obtained from the Si(111)-2×1 surface. A distinct gap of width ~0.5 eV is observed, and was identified as the gap between filled and empty surface state bands. The observation of this gap provided the first proof that localized surface states (i.e. with energies within the bulk gap) did indeed participate in the tunneling process. The corrugation amplitude of atomic rows seen in the STM images was found to be highly voltage dependent for bias voltages near the surface gap, thus relating the surface states with the observed corrugation.

With the ability of interrupting the feedback loop to maintain a fixed tip–sample separation, it is possible to scan the bias voltage continuously (as done in a spectrum) and also to quickly change the polarity of the voltage, e.g. between consecutive line scans in an image. This latter capability was important in early studies with the STM since residual drift in the microscope, and tip-related instabilities, made it difficult to compare images unless they were acquired consecutively or, even better, simultaneously. An experiment

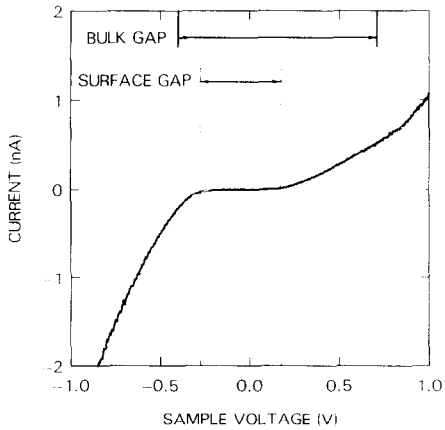

Fig. 3. Tunneling current as a function of sample voltage, measured with constant tip–sample separation on the Si(111)-2×1 surface. The 0.45 V wide flat region in the current arises from a surface state band gap, indicated together with the 1.1 V bulk band gap at the top of the figure. (From Ref. [11].)

was performed by Feenstra et al. in which the polarity of the tip–sample voltage was alternated between consecutive line scans. It was argued that the position of the observed corrugation maxima should reverse between opposite polarities for the case of the buckled model for the structure, but not for the π-bonded chain model [12]. The reversal was not seen, consistent with the latter model. Subsequent results for voltage-dependent imaging, discussed in Section 2.4 below, were more convincing since atomic features along the rows were also resolved, but the essential concept in using voltage dependence to derive structural information is provided in this early result (the same experiment had been independently suggested by Baratoff [13]).

Another method of performing tunneling spectroscopy was developed by Kaiser and Jaklevic, for their studies of Au(111) and Pd(111) surfaces [14]. In this method, the tunneling resistance is kept constant during the voltage scan, and the conductance is measured with a modulation technique. This procedure works well for metal surfaces, since a constant tunnel resistance implies a tip–sample separation which is practically constant (albeit singular at zero volts), although the method is not applicable to semiconductor surfaces since tip–sample contact would occur throughout the band gap region. Numerous features were observed in their spectra, and were interpreted in terms of the projected bulk band structure of the materials.

2.3. Current imaging tunneling spectroscopy

The method of collecting I–V curves at fixed tip–sample separation was extended by Hamers, Tromp, and Demuth to provide a powerful new method of spectroscopic imaging [15]. In the method, called current imaging tunneling spectroscopy (CITS), an I–V curve is acquired at every pixel within an image. The I–V curves themselves can be examined to reveal the spatial localization of spectral features, or images can be formed by plotting the measured current at any voltage. Furthermore, differences between current images at neighboring voltages can be plotted to enhance the spectral resolution. An example of this procedure, applied to the Si(111)7 × 7 surface, is shown in Figs. 4–6. Fig. 5 shows the total conductance (I/V) measured at various points over the 7 × 7 unit cell. Large features can be seen in the spectra, arising from specific spatial locations. For example, the onset observed near −0.8 V sample bias arises almost completely from the topographic minimum between the adatoms (i.e. from the rest atoms), whereas the onsets at −0.2 and +0.5 V arise from the adatoms. Some of these features can be visualized in the current images, shown in Fig. 4. In particular, the strong rest-atom feature with onset at −0.8 V gives rise to the maxima in the current image seen at −1.45 V in Fig. 4c. An asymmetry between the two halves of the unit cell is seen in the current image at 1.45 V, Fig. 4b, arising from surface states related to the stacking fault as seen in the conductivity spectra and images in Figs. 1 and 2.

Additional spectroscopic features of the 7 × 7 unit cell can be obtained by examining differential current images, as shown in Fig. 6. At −0.35 V, Fig. 6a, the differential current reveals the dangling bond state of the adatoms, with the faulted half of the unit cell appearing brighter. This is the same asymmetry which is typically seen in constant-current images (asymmetries in the unit cell were reported in all early STM studies [4,5,8,9], but the first clear voltage dependence of the asymmetry, with the faulted half appearing brighter at negative sample bias, was reported by Tromp et al. [16]) and these states near the Fermi level thus are responsible for that asymmetry. At large negative voltages, near −0.8 V, the rest atoms are seen as in Fig. 6b. At still higher negative voltages, Fig. 6c, features are observed which are interpreted as backbond states of the 7 × 7 structure.

It is important to understand that current images obtained with the CITS technique actually represent *difference* images, with the measured current being a difference between the current at the sampling voltage and that at the set-point voltage used for the constant-current topograph. In this sense, current images, as well as differential current images, can suffer from difficulties in interpretation in the same way as for conductivity

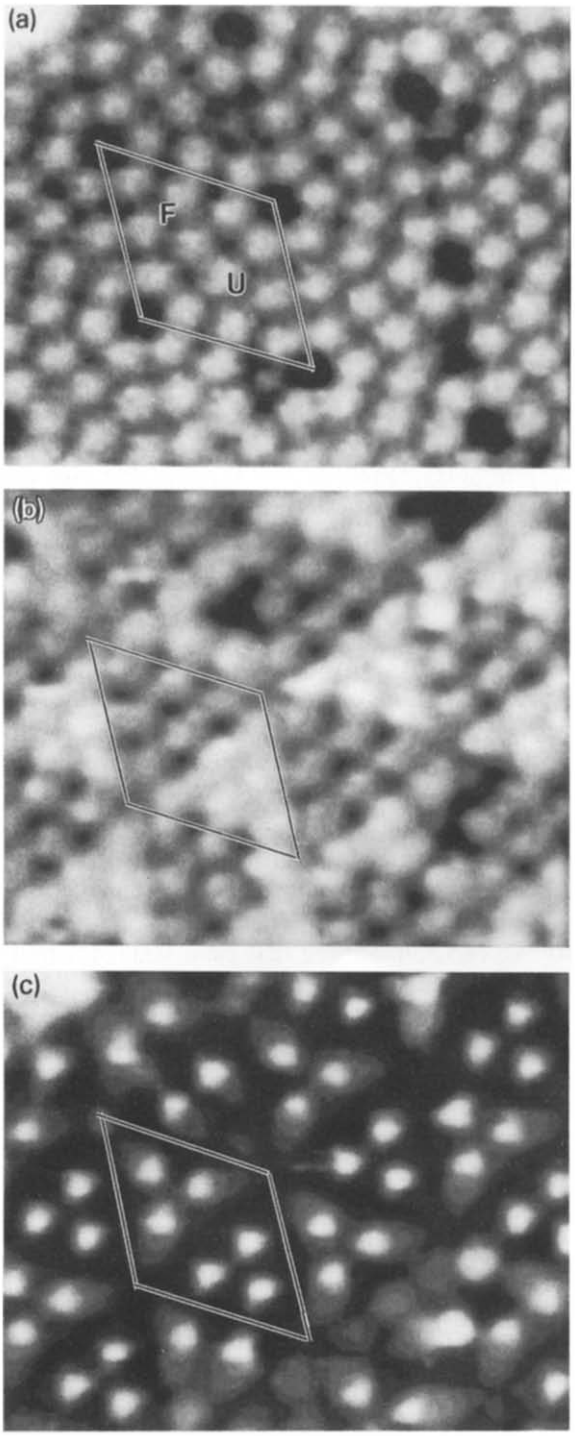

Fig. 4. Simultaneously acquired topograph and current images, for the Si(111)7×7 surface: (a) STM topograph with +2 V sample voltage, and current images with (b) +1.45 V and (c) −1.45 V applied to the sample. (From Ref. [15].)

images, discussed in Sections 2.1 and 3. Any type of spectroscopic image can be dominated by certain background features of the spectroscopy rather than genuine surface state features. This property of CITS imaging was examined by Hamers and co-workers [15,16], who argued that in cases where the topograph reflected mainly *geometric* features of the surface, then the current images would contain predominantly *electronic* information. This argument does have some qualitative basis for those systems in which it is possible to find such a topograph, but it is not possible to know a priori whether a given constant-current image does indeed contain predominantly geometric information. Subsequent work, discussed below, demonstrated that electronic ef-

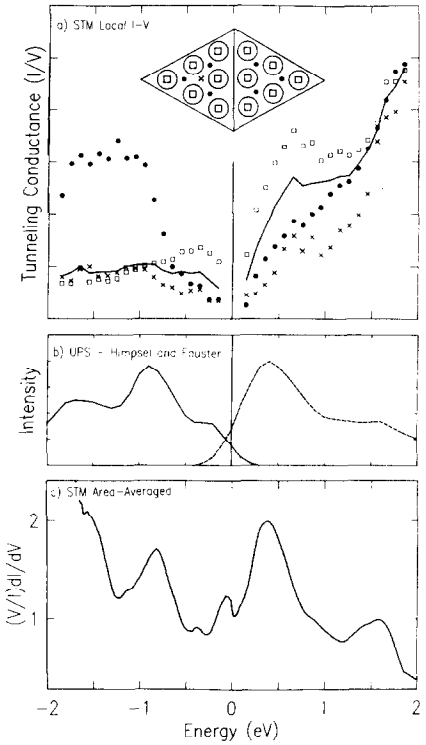

Fig. 5. (a) Constant-separation $\sigma - V$ spectra for the Si(111)-7×7 surface averaged over one unit cell (solid line) and at selected locations in the unit cell (other symbols). Crosses are from the faulted half only; others are averaged over both halves of the unit cell. (b) Surface observed using ultraviolet photoemission (solid line) and inverse photoemission (dashed line), from Refs. [47,48]. (c) Area-averaged spectroscopy results. (Adapted from Ref. [15].)

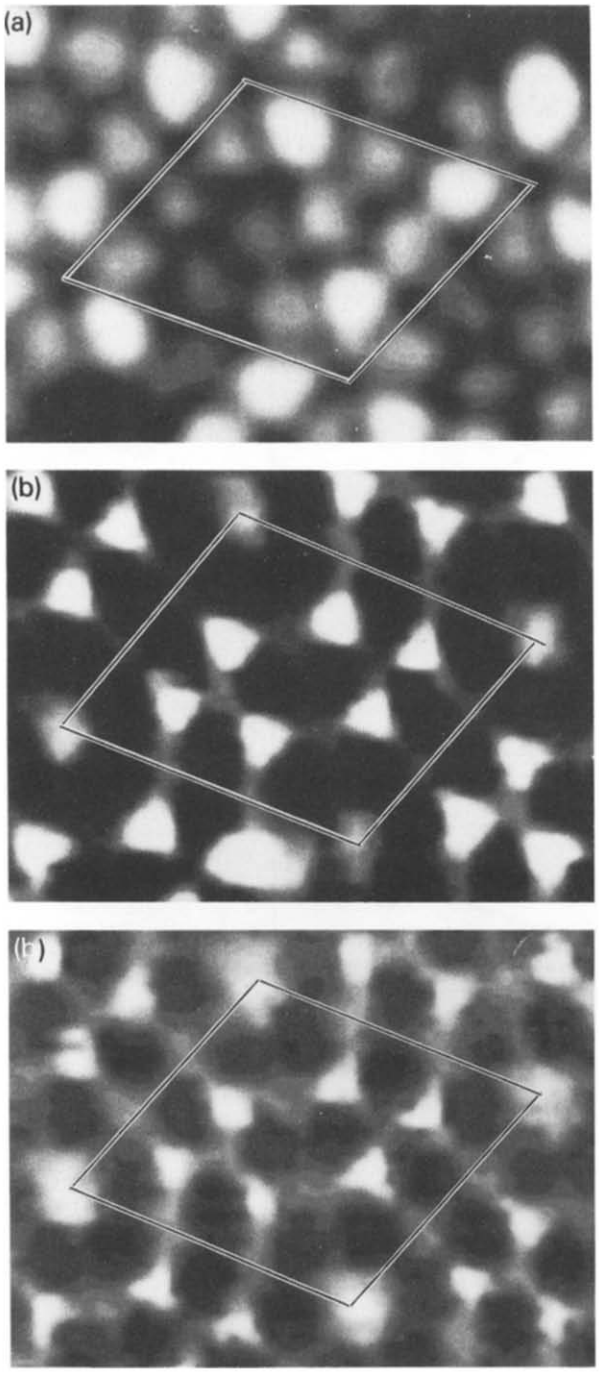

Fig. 6. CITS images of occupied Si(111)7×7 surface states. (a) Adatom state at −0.35 V, (b) dangling bond state at −0.8 V, and (c) backbond state at −1.7 V. (From Ref. [15].)

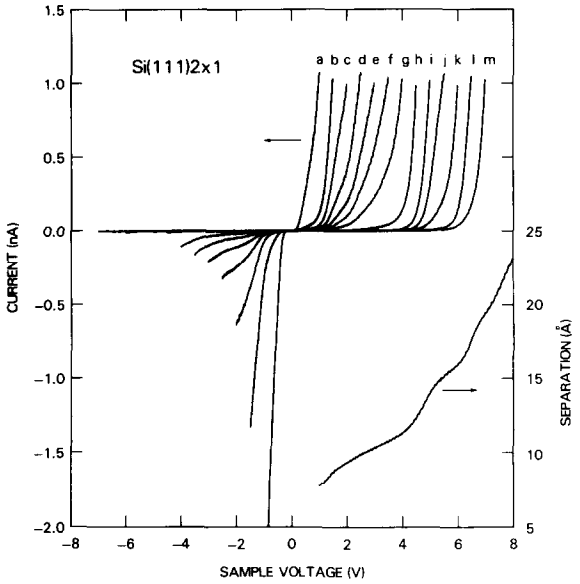

Fig. 7. Tunneling current vs. voltage for a tungsten probe-tip and Si(111)2×1 sample, at tip–sample separations of 7.8, 8.7, 9.3, 9.9, 10.3, 10.8, 11.3, 12.3 14.1, 15.1, 16.0, 17.7, and 19.5 Å for the curves labelled a–m, respectively. These separations are obtained from a measurement of separation vs. voltage, at 1 nA constant current, shown in the lower part of the figure. (From Ref. [17].)

fects can and do play an important role in STM imaging at all voltages, and a simple separation between electronic and geometric effects cannot generally be obtained. On the other hand, by understanding the electronic properties of a given structure, it is often possible to use some type of voltage-dependent or spectroscopic imaging to directly confirm or deny specific structure models.

2.4. Spectroscopic normalization and polarity-dependent imaging

Subsequent work by Stroscio, Feenstra and Fein on the Si(111)2×1 surface provided new results in two areas of STM spectroscopic research [17]. First, detailed I–V measurements at a variety of different tip–sample separations were performed, as shown in Fig. 7. Surface state-density features can be seen in these I–V curves as the various kinks and bumps occurring between −4 and 4 V. The features are obscured by the

fact that the tunneling current depends exponentially on both separation and voltage. It was found that this dependence could be effectively removed by plotting the ratio differential to total conductance, $(dI/dV)/(I/V)$, as shown in Fig. 8b where the different symbols refer to different curves from Fig. 7 (this same type of normalization was also used effectively by Lang, in his theoretical studies of metal adsorbates [18]). A detailed spectrum of states is thus obtained, and good agreement was found between the measurements and theoretical expectations for the π-bonded chain model, shown in Fig. 8c. In addition, the inverse decay length of the tunnel current could be extracted from the data, shown in Fig. 8a, and for low voltages near the surface state band edges, this showed an enhancement over the usual values of $\sqrt{(2m\phi/\hbar^2)} \simeq 1.1$ Å^{-1}.

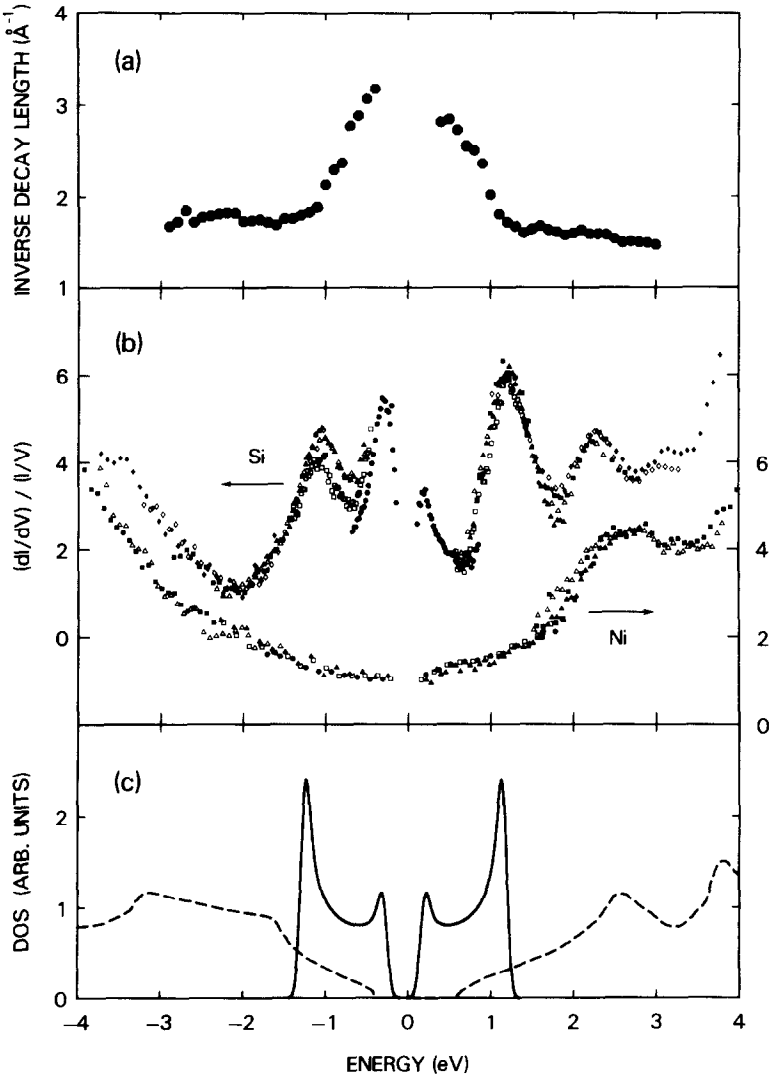

Fig. 8. (a) Inverse decay length of the tunneling current as a function of energy (relative to the surface Fermi level), for the Si(111)2 × 1 surface. (b) Ratio of differential to total conductivity for silicon and for nickel. The different symbols refer to different tip–sample separations. (c) Theoretical DOS for the bulk valence band and conduction band of silicon (dashed curve, Ref. [49]), and the DOS from a one-dimensional tight-binding model of the π-bonded chains (solid line, Ref. [50]). (From Ref. [17].)

In addition, Stroscio and co-workers presented dramatic new results for the voltage dependence of the Si(111)2 × 1 STM images. Images were acquired at voltages on either side of the surface band gap. As shown in Fig. 9, each image shows a single topographic maxima per 2 × 1 unit cell. However, the position of this maxima was found to shift by one-half a unit cell (1.92 Å) in the [0$\bar{1}$1] direction when the polarity of the voltage was changed. A smaller shift of 0.7 Å was found for the orthogonal [2$\bar{1}\bar{1}$] direction. This voltage dependence of the images was easily interpreted in terms of the surface state band structure for the π-bonded chain model: the surface band gap

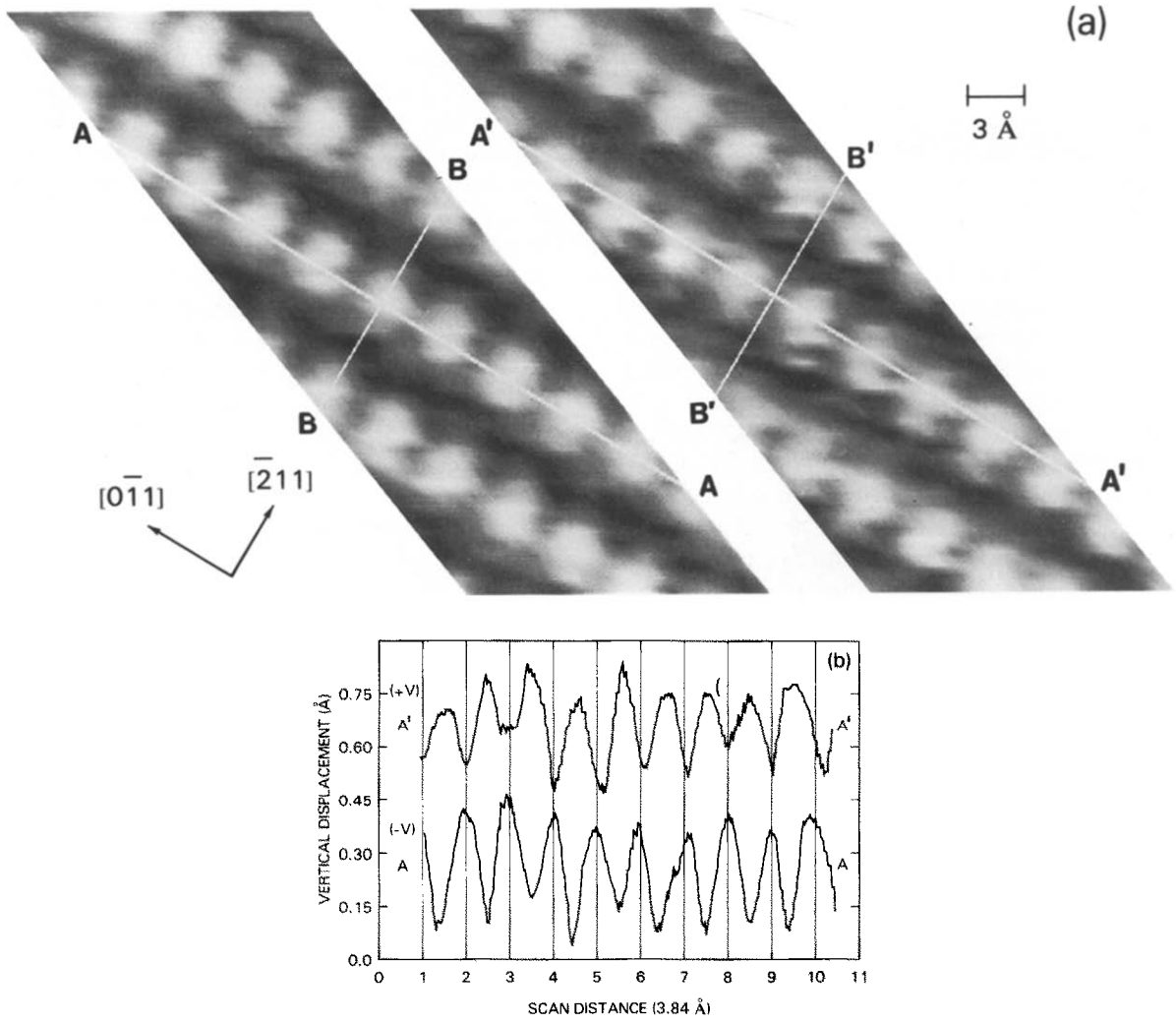

Fig. 9. Constant-current STM image acquired from the Si(111)2 × 1 surface at sample voltages of −0.7 and +0.7 V for the left and right images, respectively. The surface height is given by a grey-scale, ranging from 0 Å (black) to ~ 1 Å (white). (b) Surface height along the cross-sections AA and A'A', which occur at identical lateral positions in the two images. The curve A'A' has been shifted 0.5 Å upwards relative to AA, and the zero level on the y axis is arbitrary. Maxima in one cross-section correspond to minima in the other. (From Ref. [17].)

formed due to the inequivalence of the two silicon atoms in the surface unit cell, and at the band edges the wave-function was localized entirely on one or the other of the atoms. Thus, the images provided a direct connection to the electronic properties of the surface structure. Other models for the 2×1 structure were not consistent with the observed voltage dependence [11,17].

The work of Stroscio et al. provided the first clear demonstration that the STM actually imaged surface wave-functions rather than just atomic positions. At the time, it was of course known from theoretical considerations that the tunnel current consisted of the overlap of wave-functions between tip and sample, and, neglecting details of the tip, the images could be interpreted as the local state-density of the sample surface [19]. Nevertheless, it was still quite tempting to think that geometric features on the surface might dominate the images, and this viewpoint was advanced with the studies of the Si(111)7×7 surface discussed above. The new results for the Si(111)2×1 surface demonstrated conclusively that the simple interpretation in terms of geometric positions was invalid for any applied bias between tip and sample – electronic effects dominated the images. However, these electronic effects could be used to advantage in deducing the underlying structure of the surface; since the electronic properties of most simple surface can be constructed based on elementary considerations, it was still possible in many cases to directly confirm or deny specific structural models.

2.5. *Other studies*

From the above studies of the Si(111)7×7 and Si(111)2×1 surfaces, the major concepts of STM surface state spectroscopy were deduced. Subsequent studies of other surfaces provided additional emphasis of these concepts. For clean surfaces, the Si(001)2×1 surface had been studied early on in terms of its basic topography (symmetric or asymmetric dimers) [20], and voltage dependence of this surface was reported by Hamers, Tromp and Demuth [21]. A distinct minimum in the corrugation for the empty states directly on top of the dimers was seen in both constant-current images and CITS current images, and was interpreted in terms of the node which occurs for these anti-bonding states.

The study of adsorbates on surfaces provided important new results which could be compared and contrasted with the prior studies of clean surfaces. The first adsorbate system to be studied, the $(\sqrt{3} \times \sqrt{3})$R30° structure of Ag on Si(111), turned out to be controversial since two STM groups came to different conclusions regarding the structure. Using constant-current images with positive sample bias, Wilson and Chiang observed the $\sqrt{3} \times \sqrt{3}$ structure with two topographic maxima per unit cell [22]. A simple honeycomb model, in which the observed topographic maxima corresponded to Ag atoms on the surface, was found to match the data so long as electronic effects in the images were small. The same surface was studied by van Loenen, Demuth, Tromp, and Hamers using the CITS method [23]. A similar honeycomb STM image was obtained for small negative sample biases, but for larger negative biases the corrugation was substantially reduced. CITS images at positive bias also revealed the honeycomb structure, and a surface state gap between empty and filled states was observed. It was argued that the data supported an embedded Ag-trimer, Si-honeycomb model, in which the Ag layer was embedded below a top Si layer, and the Si atoms in this top layer formed the honeycomb pattern which was seen in STM. The controversy was fueled by a subsequent STM study by Wilson and Chiang [24]. Investigations of this surface by many other techniques finally led to the proposal of a honeycomb-chained-trimer (HCT) model in which the top layer consists of Ag atoms in the HCT arrangement, below which there is a layer of Si atoms which form trimers [25]. Theoretical calculations revealed that the empty states for this structure did indeed form a honeycomb arrangement, but the maxima are not associated with individual surface atoms [26]. Rather, the corrugation maxima for empty states occurs in the middle of Ag trimers on the surface. Thus, agreement between the STM images and all other methods was finally achieved, as discussed in a reexamination of this surface by STM [27].

Although a careful examination of the voltage dependence of the STM images for Si(111)–Ag does yield results which are consistent with the known structure [27], it would be presumptuous to think that the STM could have determined this structure originally. Indeed, much of the voltage dependence was already known from the work of van Loenen et al., and furthermore, the possibility of the observed topographic maxima corresponding to Ag trimers had been considered by Wilson and Chiang. This latter possibility was rejected based on the arrangement of trimers for the simple model they considered, thus illustrating an intrinsic limitation of the STM for structural determination of complicated structures: if extensive reconstruction exists below the top surface layer, it is difficult on the basis of STM images alone to uniquely determine the geometric structure.

One clean surface structure which had been important in the development of low-energy electron diffraction techniques was the buckled geometry of GaAs(110). The basic topography of this surface had been observed in an early STM study [28], and the voltage dependence of the images was reported by Feenstra, Stroscio, Tersoff and Fein [29]. Empty states on the surface were found to be localized over the Ga atoms, and filled states over the As atoms, thus confirming an earlier theoretical prediction for this surface [19]. The spatial separation between empty and filled states provided a quantitative measure of the surface buckling. This situation for GaAs(110) is analogous to that observed earlier on Si(111)2×1, although the contrast between the two atoms in the unit cell arises, for Si, from a structural inequivalence, whereas for GaAs it comes, of course, from the fact that they are different atoms with As being more electronegative than Ga.

Numerous STM studies of clean and adsorbate covered surfaces followed these early works. The subsequent studies served to reinforce the concepts which had been developed in the initial investigations. We mention one study here, on the Ge(111)c(2×8) surface, which settled some of the controversy that had developed in earlier studies of Si(111)7×7 and Si(111)2×1. As discussed above, the STM topographs for Si(111)-7×7 had been interpreted primarily in terms of geometric structure, whereas the topographs for Si(111)2×1 were found to consist primarily of electronic structure. This difference arises, of course, in large part from the different structures of the two surfaces: the 7×7 structure contains adatoms (located ~ 1 Å above the underlying layer) which are significant geometric features, whereas the 2×1 is relatively flat (along the π-bonded chains) and thus dominated by electronic effects. The c(2×8) structure provides an interesting comparison, since it also contains adatoms, but the charge transfer between adatoms and rest atoms is complete so that a surface state band gap exists thereby implying possibly large electronic effects. The basic topography of the Ge(111)c(2×8) surface was observed in an early STM work [30], and a detailed study of the spectroscopy and voltage dependence was presented by Becker and co-workers [31]. It was found that the topographic maxima in the images shift their positions between filled and empty states. The adatoms are seen in the filled state images, but despite the geometric protuberance of the adatoms the empty state images show a minimum in topography at the adatom sites. Thus, it was concluded that electronic effects dominate in the images. The STM images could essentially be understood in a "dangling bond picture", based on the earlier studies of Si(111)2×1 and GaAs(110): the major source of contrast in all types of STM images of semiconductor surfaces comes from states associated with the surface dangling bonds, and such states are seen only at the specific bias voltages which access their energy levels.

Many subsequent STM works yielded spectroscopic information on new systems, and also reproduced the original early results. Examples of the latter include: for Si(111)7×7 and related systems, observation of the stacking fault states in conductance spectroscopy [32], and observation of the adatom and rest atom derived states by constant-separation spectroscopy [33,34]. The spectrum of states for Si(111)2×1 was reproduced [35,36], and similar observations were made on the Ge(111)2×1 surface [36]. The above-men-

tioned results for Ge(111)c(2 × 8) were also reproduced [37]. Thus, all of the early results survived the test of time, and they formed a reliable base on which to build an understanding of STM spectroscopy.

3. Discussion

In this section, we analyze and compare the various methods developed for acquiring spectra with the STM. For semiconductor surfaces, a very important feature of such measurements is their *dynamic range*. To fully resolve all the features in a spectrum acquired with constant tip–sample separation over the voltage range of, say, −3 to 3 V requires a dynamic range in the current or conductance of 4–6 orders-of-magnitude, with the higher values required in cases where the surface state band gap is large. Such a large variation in the current originates, at high voltages, from the voltage dependence of the tunneling transmission probability, and at low voltages from the varying state-density of the semiconductor itself. Measurement of such a wide range of current values is practically impossible in a single I–V curve, since the integration time for the measurement is limited because of residual drift in the STM. Fortunately, the STM allows us to overcome this limitation simply by varying the tip–sample separation, thereby amplifying the current at low voltages and permitting measurement of the entire spectrum with the experimentally available dynamic range.

These issues regarding dynamic range can be clearly seen in the results reviewed in Section 2. For example, for the Si(111)7 × 7 surface we compare the spectrum in Fig. 2 with that in Fig. 5. The former is dI/dV acquired at constant I, thereby allowing observation at large voltages, but not permitting measurement through zero volts nor at low voltages less than about 1 V (the conductance at constant current diverges at low voltages). The latter is I/V acquired at constant tip–sample separation, so that the spectrum is limited to voltages less than about 2 V. In the region of overlap, the same features are observed (peak I in Fig. 2, observed as the onset at 1.5 V in Fig. 5), but clearly neither spectrum displays all the spectral information. Turning now to the results of Figs. 7 and 8, it was found that multiple I–V curves at various tip–sample separations could yield the entire spectrum with high spectral resolution. Note that although each measurement was performed at constant tip–sample separation, the subsequent normalization relied on using the ratio of conductance to current, thus mimicking the constant-current measurement! This interplay between constant current versus constant separation, and the issue of dynamic range which is especially vexing for wide band gap surfaces such as GaAs(110), was explored in a series of subsequent works [38]. In this author's opinion most of the issues regarding acquisition and analysis techniques are now understood, although admittedly, application of these techniques is not widespread.

Let us now consider what is arguably the most powerful aspect of the STM – spatially resolved spectroscopic measurement or spectroscopic imaging. Three methods for spectroscopic images have been reviewed in Section 2: conductance imaging, current (or differential current) imaging in the CITS mode, and voltage dependent imaging. To the casual reader it might appear that the results from any of these techniques are essentially equivalent, and it should be possible to easily transform data from one method into another. This is, however, definitely not the case! On the contrary, images obtained by these methods often yield contradictory results, and phenomenon such as contrast reversal (maxima in images appearing where the atoms or electron are *not* localized) can be easily obtained, as has been discussed in detail for the Si(111)7 × 7 and 2 × 1 surfaces [33,39,40]. The essential problem in spectroscopic imaging is illustrated in Fig. 10, where we plot a typical I–V curve which might be obtained over two spatial locations on a surface [41]. In the example shown, the currents are equal at V_1, which could be the constant-current setpoint, and the I–V curves are measured at the constant tip–sample separation determined by this setpoint. In curve (a), a large spectral feature is seen at V_2, which is not present in curve (b). Thus, a current image obtained in the CITS mode

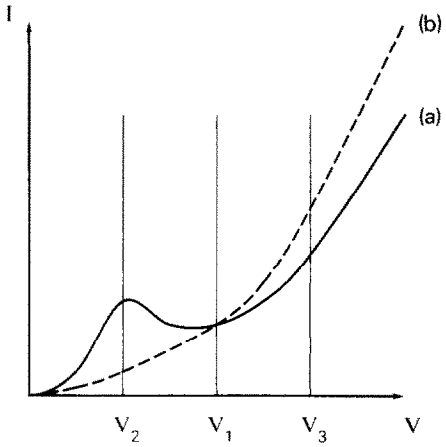

Fig. 10. Schematic illustration of current–voltage characteristics at two different spatial locations (a) and (b) on a surface. The currents are equal at the voltage V_1. At V_2, a surface-state feature appears at location (a), and it can be imaged at that voltage. An image formed at the voltage V_3 will show a maximum at spatial location (b), associated with the varying background level of the current. (From Ref. [41].)

would correctly spatially resolve this feature. However, a current image performed at some other voltage, say V_3 would produce spatial maxima over position (b). In this case, the maxima arise purely from the varying background level of the tunnel current, and have nothing to do with any real spatially resolved spectral feature. Similar comments can be made for differential current images, or for conductance images acquired at constant current. In cases where the spectral features are large, then all of the methods will produce correct spectroscopic images, but when the features are small (or nonexistent) then care must be used in the interpretation of the images.

The above problems of artifacts in spectroscopic imaging are minimized when one considers simply the voltage dependence of constant-current images. Since the tunnel current consists of contributions integrated over the entire energy range between the tip and sample Fermi levels, it is explicitly *not* a difference measurement, and thus it is less sensitive to possible background effects. On the other hand, this feature of constant-current images will, of course, produce less spectral resolution in the images. However, one particular aspect of constant-current images has turned out to provide a powerful and general method for structural analysis, that is, comparing images obtained with positive and negative bias voltages. For surfaces which possess an energy band gap in their state-density (which is practically all semiconductor surfaces, with the exception of Si(111)7 × 7), images of filled and empty states, obtained near the band edges, often contain significant structurally dependent features. This proved to be an essential feature in STM structural determination for the Si(111)2 × 1 surface, discussed above. Even for the case of the Si(111)7 × 7 surface, in which the polarity dependence is not so striking because of the partially filled adatom states, the surface stacking fault is directly seen in the voltage dependence (the rest atoms can also be seen directly in voltage dependent imaging [31,42], although not nearly as well as can be achieved with the CITS imaging). And particularly for the case of Si(111)–Ag, it is seen above that the voltage dependence of the STM images does contain the essential structural information, which cannot be obtained by examining single topographs.

4. Summary

In this paper, we have reviewed the history of STM spectroscopy, with emphasis on the strengths and weaknesses of spectroscopic imaging as applied to surface structural determination. It is perhaps appropriate at this point to remind ourselves of the comment made in Section 1, that structural determination is only one small part of the range of application for STM spectroscopy. As illustrations of this point, we note the recent application of current imaging to the observation of band gap states induced by metal adsorbates on the GaAs(110) surface [43]. The CITS method is ideally suited to this study, since the tunnel current is zero at all locations other than around the adsorbates. Similarly, conductance imaging has proved to be ideally suited to several recent studies involving purely spectroscopic (nonstructural) features of the surface [44,45]. Finally, to generalize our scope even more, it should be remembered that STM spectroscopic measure-

ment forms only one small area of application of the STM technique itself. Even for semiconductor surfaces, where spectroscopy finds its major application, the multitude of recent studies involving, e.g., epitaxial growth on surfaces [46], demonstrates the wide and major application of STM in areas where spectroscopic effects are small. Thus, the range of STM applications is very large, and in this work we have described one small, but powerful, application of the scanning tunneling microscope.

Acknowledgements

The author acknowledges many friends and co-workers who have provided insight into areas of STM spectroscopy. In particular, I am grateful for a collaboration with Joseph A. Stroscio during the early years of development of this field.

References

[1] G. Binnig, H. Rohrer, Ch. Gerber and E. Weibel, Appl. Phys. Lett. 40 (1982) 178.
[2] G. Binnig, H. Rohrer, Ch. Gerber and E. Weibel, Phys. Rev. Lett. 49 (1982) 57.
[3] G. Binnig and H. Rohrer, Helv. Phys. Acta 55 (1982) 726.
[4] G. Binnig, H. Rohrer, Ch. Gerber and E. Weibel, Phys. Rev. Lett. 50 (1983) 120.
[5] G. Binnig, H. Rohrer, F. Salvan, Ch. Gerber and A. Baro, Surf. Sci. 157 (1985) L373.
[6] R.S. Becker, J.A. Golovchenko and B.S. Swartzentruber, Phys. Rev. Lett. 55 (1985) 987.
[7] G. Binnig, K.H. Frank, H. Fuchs, N. Garcia, B. Reihl, F. Salvan and A. R. Williams, Phys. Rev. Lett. 55 (1985) 991.
[8] R.S. Becker, J.A. Golovchenko, D.R. Hamann and B.S. Swartzentruber, Phys. Rev. Lett. 55 (1985) 2032.
[9] R.S. Becker, J.A. Golovchenko, D.R. Hamann and B.S. Swartzentruber, Phys. Rev. Lett. 55 (1985) 2028.
[10] K. Takayanagi, Y. Tanishiro, M. Takahashi and S. Takahashi, J. Vac. Sci. Technol. A 3 (1985) 1502.
[11] R.M. Feenstra, W.A. Thompson and A.P. Fein, Phys. Rev. Lett. 56 (1986) 608.
[12] K.C. Pandey, Phys. Rev. Lett. 47 (1981) 1913; 49 (1982) 223.
[13] A. Baratoff, Physica B 127 (1984) 143.
[14] W.J. Kaiser and R.C. Jaklevic, IBM J. Res. Dev. 30 (1986) 411.
[15] R.J. Hamers, R.M. Tromp and J.E. Demuth, Phys. Rev. Lett. 56 (1986) 1972.
[16] R.M. Tromp, R.J. Hamers and J.E. Demuth, Phys. Rev. B 34 (1986) 1388.
[17] J.A. Stroscio, R.M. Feenstra and A.P. Fein, Phys. Rev. Lett. 57 (1986) 2579.
[18] N.D. Lang, Phys. Rev. B 34 (1986) 5947.
[19] J. Tersoff and D.R. Hamann, Phys. Rev. Lett. 50 (1983) 1998; Phys. Rev. B 31 (1985) 805.
[20] R.M. Tromp, R.J. Hamers and J.E. Demuth, Phys. Rev. Lett. 55 (1985) 1303.
[21] R.J. Hamers, R.M. Tromp and J.E. Demuth, Surf. Sci. 181 (1987) 346.
[22] R.J. Wilson and S. Chiang, Phys. Rev. Lett. 58 (1987) 369.
[23] E.J. van Loenen, J.E. Demuth, R.M. Tromp and R.J. Hamers, Phys. Rev. Lett. 58 (1987) 373.
[24] R.J. Wilson and S. Chiang, Phys. Rev. Lett. 59 (1987) 2329.
[25] A. Ichimiya, S. Kohmoto, T. Fujii and Y. Horio, Appl. Surf. Sci. 41/42 (1989) 82;
M. Katayama, R.S. Williams, M. Kato, E. Nomura and M. Aono, Phys. Rev. Lett. 66 (1991) 2762.
[26] Y.G. Ding, C.T. Chan and K.M. Ho, Phys. Rev. Lett. 67 (1991) 1454;
S. Watanabe, M. Aono and M. Tsukada, Phys. Rev. B 44 (1991) 8330.
[27] K.J. Wan, X.F. Lin and J. Nogami, Phys. Rev. B 45 (1992) 9509.
[28] R.M. Feenstra and A.P. Fein, Phys. Rev. B 32 (1985) 1394.
[29] R.M. Feenstra, J.A. Stroscio, J. Tersoff and A.P. Fein, Phys. Rev. Lett. 58 (1987) 1192.
[30] R.S. Becker, J.A. Golovchenko and B.S. Swartzentruber, Phys. Rev. Lett. 54 (1985) 2678.
[31] R.S. Becker, B.S. Swartzentruber, J.S. Vickers and T. Klitsner, Phys. Rev. B 39 (1989) 1633.
[32] R.S. Becker, B.S. Swartzentruber and J.S. Vickers, J. Vac. Sci. Technol. A 6 (1988) 472.
[33] Th. Berghaus, A. Brodde, H. Neddermeyer and St. Tosch, Surf. Sci. 193 (1988) 235.
[34] R. Wolkow and Ph. Avouris, Phys. Rev. Lett. 60 (1988) 1049.
[35] R.S. Becker, T. Klistner and J.S. Vickers, Phys. Rev. B 38 (1988) 3537.
[36] R.M. Feenstra, Phys. Rev. B 44 (1991) 13791.
[37] R.M. Feenstra and A.J. Slavin, Surf. Sci. 251/252 (1991) 401.
[38] For a review, see J.A. Stroscio and R.M. Feenstra, in: Scanning Tunneling Microscopy, Eds. J.A. Stroscio and W.J. Kaiser (Academic, Boston, MA, 1993) ch. 4.
[39] G. Binnig and H. Rohrer, IBM J. Res. Dev. 30 (1986) 355.
[40] J.A. Stroscio, R.M. Feenstra, D.M. Newns and A.P. Fein, J. Vac. Sci. Technol. A 6 (1988) 499.

[41] R.M. Feenstra, in: Scanning Tunneling Microscopy and Related Methods, Eds. R.J. Behm, N. Garcia and H. Rohrer (Kluwer, Dordrecht, 1990).
[42] Ph. Avouris and R. Wolkow, Phys. Rev. B 39 (1989) 5091.
[43] J.A. Stroscio, P.N. First, R.A. Dragoset, L.J. Whitman, D.T. Pierce and R.J. Celotta, J. Vac. Sci. Technol. A 8 (1990) 284.
[44] J.A. Kubby, Y.R. Wang and W.J. Greene, Phys. Rev. Lett. 65 (1990) 2165.
[45] A. Vaterlaus, R.M. Feenstra, P.D. Kirchner, J.M. Woodall and G.D. Pettit, J. Vac. Sci. Technol. B 11 (1993) 1502.
[46] For example, Y.W. Mo, J. Kleiner, M.B. Webb and M.G. Lagally, Phys. Rev. Lett. 66 (1991) 1998.
[47] F.J. Himpsel and Th. Fauster, J. Vac. Sci. Technol. A 2 (1984) 815.
[48] Th. Fauster and F.J. Himpsel, J. Vac. Sci. Technol. A 1 (1993) 1111.
[49] J.R. Chelikowsky and M.L. Cohen, Phys. Rev. B 10 (1974) 5095.
[50] R. Del Sole and A. Selloni, Phys. Rev. B 30 (1984) 883.
[51] H. Rohrer, Surf. Sci. 299/300 (1994) 956.